Journal of
Materials Chemistry C

ROYAL SOCIETY OF CHEMISTRY

PAPER

View Article Online
View Journal | View Issue

Published on 01 December 2015. Downloaded by South China University of Technology on 25/02/2016 06:24:13.

Cite this: *J. Mater. Chem. C*, 2016, 4, 362

Monolayer hexagonal arsenene with tunable electronic structures and magnetic properties *via* impurity doping†

Zhongjun Li,[a] Wei Xu,[a] Yuanqin Yu,[b] Hongyang Du,[a] Kun Zhen,[a] Jun Wang,[a] Linbao Luo,*[a] Huaili Qiu[a] and Xiaobao Yang*[c]

Received 19th September 2015, Accepted 30th November 2015

DOI: 10.1039/c5tc03001c

www.rsc.org/MaterialsC

Monolayer hexagonal arsenene (hAs), a typical two-dimensional semiconducting material with a wide band gap and high stability, has attracted increasing research interest due to its potential applications in optoelectronics. Using first-principles calculations, we have investigated the electronic and magnetic properties of x-substituted hAs (x = B, C, N, O, Ga, Ge, Se, and monovacancy) and x-adsorbed hAs (x = As). Our results show that the B-, N-, and Ga-substituted hAs have spin-unpolarized semiconducting characters like pristine hAs, and indirect–direct band gap transitions are induced in the B- and N-substituted systems. In contrast, the O-, Se-, and monovacancy-substituted hAs are metallic, and the C- and Ge-substituted hAs show spin-polarized semiconducting characters with band gaps of 1.1 and 1.3 eV for the spin-up channels and 1.0 and 0.7 eV for the spin-down channels, respectively. For the As-adsorbed hAs, the Fermi level crosses the spin-up states, yielding metallic behavior, while the spin-down channel retains semiconducting character. Detailed analysis of electronic structures for the C-substituted, Ge-substituted, and As-adsorbed hAs shows that strong hybridizations between the doping atoms and As atoms lead to energy splitting near the Fermi level and consequently induce magnetic moments. By selective doping, hAs can be transformed from a spin-nonpolarized semiconductor to a spin-polarized semiconductor, to a half-metal, or even to a metal, which indicates that the doped hAs will have promising potential in future electronics, spintronics, and optoelectronics.

1. Introduction

Due to the integration limit of silicon-based devices, more and more attention has been paid to two-dimensional (2D) materials, such as graphene,[1,2] silicene,[3,4] boron nitride,[5–7] transition metal dichalcogenides,[8–10] and black phosphorus,[11–13] due to their rather unique properties. The atomic level thickness of these materials leads to substantially novel performances in electronic structures. For example, a transition of indirect–direct band gaps occurs when MoS_2 changes from multilayered or bulk to a monolayered structure.[9] Furthermore, the devices based on these 2D materials show small short channel effects and excellent electrostatic modulations because of their ultrathin thickness. Therefore, in recent years, many high-performance electronic and optoelectronic devices based on these 2D materials have been developed.[10–17]

[a] School of Electronic Science and Applied Physics, Hefei University of Technology, Hefei, Anhui 230009, China. E-mail: luolb@hfut.edu.cn
[b] School of Physics and Material Science, Anhui University, Hefei, Anhui 230039, China
[c] Department of Physics, South China University of Technology, Guangzhou, Guangdong 510641, China. E-mail: scxbyang@scut.edu.cn

† Electronic supplementary information (ESI) available. See DOI: 10.1039/c5tc03001c

Recently, two studies on 2D arsenene sheets were performed using first-principles calculations. Zhang *et al.* predicted two types of 2D materials, monolayer hexagonal arsenene (hAs) and antimonene (hSb), which exhibit typical semiconducting characteristics with high stability and wide indirect band gaps of 2.49 and 2.28 eV, respectively.[18,19] Moreover, under small biaxial strain, these two materials were found to transform from indirect into direct band gap.[18] Kamal *et al.* systematically investigated the stability and electronic properties of the arsenic system, including buckled and puckered honeycomb structures, both of which possess indirect gaps and undergo an indirect-to-direct band gap transition by applying strain.[19] Such essential changes in electronic structures will facilitate the fabrication of transistors with high on/off ratio, optoelectronic devices, and mechanical sensors.[18,19]

Due to the potential applications, more recently, several theoretical studies on hAs and its analogs have been performed in an effort to tune their electronic properties.[20–24] For example, Kou *et al.* studied the geometric structures, electronic properties, and external strain deformation effect of hAs and antimony arsenide.[20] It was revealed that both materials are indirect band semiconductors, and an indirect–direct band gap transition can

 This journal is © The Royal Society of Chemistry 2016

Published on 01 December 2015. Downloaded by South China University of Technology on 25/02/2016 06:24:13.

be achieved when a small tensile strain is applied.[20] On the basis of first-principles calculations, Wang *et al.* found that for hAs and hSb sheets, the armchair nanoribbons are indirect semiconductors while the zigzag nanoribbons are direct ones regardless of the ribbon width.[21]

It is noted that, despite the huge progress mentioned above, the means to tune the electronic structures of hAs and hSb are limited to exerting external strain on the sheets or cutting them into nanoribbons, which are difficult in practice. As is known, doping is a feasible method for modifying electronic and magnetic properties of semiconducting materials, such as MoS_2,[25–27] hBN,[28–30] germanium,[31,32] and so on. It has been recognized that practically stable doping requires substitution of host atoms, where the doping is secured through covalent bonding. For hAs and hSb sheets, doping is highly desirable as the tailoring of their electrical properties is paramount to their device applications. Therefore, considering the larger band gap in hAs than that in hSb sheets, we have theoretically investigated the possibility to tune the electronic structures and magnetic properties of hAs by substitutional doping with various atoms of B, C, N, O, Ga, Ge, and Se. In addition, the doping of monovacancies and adsorption of As atoms have also been investigated because these two types of impurities may occur in the preparation of hAs.

In the present work, the structural stabilities, electronic structures, and magnetic properties of x-substituted hAs (x = B, C, N, O, Ga, Ge, Se, and monovacancy) and x-adsorbed hAs (x = As) have systematically been studied based on first-principles calculations. The influences of doping on the geometric structures are evaluated by comparing the structural parameters for the systems before/after doping. On the basis of the optimized geometric structures, formation energies, magnetic moments, and charge transfers from doping atoms to hAs are obtained. For all doped systems, the conducting characteristics are emphatically studied on the basis of the spin-polarized band structures and partial density of states (PDOS). This work will explore the possibility of tuning the electronic properties of arsenene sheets, as well as other 2D systems, by appropriate atomic doping.

2. Computational methods

The first-principles calculations were performed based on density functional theory (DFT) implemented in the Vienna ab initio simulation package (VASP).[33–35] The exchange correlation potential was approximated by the generalized gradient approximation (GGA) with the PBE functional.[36] Electronic wave functions were expanded using a plane-wave basis set with a cutoff energy of 550 eV. A 4 × 4 supercell consisting of 16-fold unit cells of hAs was used with a vacuum space of 15 Å to eliminate the cell-to-cell interactions. One B, C, O, Ga, Ge, and Se atom each was used to substitute one As atom in the supercell, respectively. Moreover, the monovacancy and the adsorption of an isolated As atom were also considered in the supercell. The impurity concentration is 1/32. The test calculation was also carried out for a 6 × 6 supercell with a smaller concentration, and the main results, as shown in Fig. S1 in the ESI,† remain unchanged. Therefore, all the theoretical simulations were carried out with the 4 × 4 supercell. The Monkhorst–Pack *k*-point samplings in the Brillouin zone are 7 × 7 × 1 and 13 × 13 × 1 meshes in the optimization of geometrical structures and in the calculation of electronic structures, respectively. The full-relaxation of structures with spin-nonpolarized and spin-polarized calculations were carried out until the force components were smaller than 0.01 eV Å^{-1}, and the convergence criteria is 10^{-4} eV for energy. Bader analysis was used to calculate the charge transfer.[37] To evaluate the stability of the doped systems, the energy of formation is defined as $E_f = E_{complex} + E_{As} - (E_{hAs} + E_x)$, where $E_{complex}$ and E_{hAs} are the total energies of the doped and the pristine hAs systems, and E_{As} and E_x are the energies of the atoms in their bulk form except for the cases in which the energies of x atoms (x = N and O) in their molecular gas phase are employed. By including the spin–orbit coupling effects in the calculations, we found that these effects on band structures of the doped systems can be neglected, as shown in Fig. S2 and S3 (ESI†). Therefore, the spin–orbit coupling effects are not included in the following calculations.

3. Results and discussion

3.1 x-Substituted hAs (x = B, C, N, O, Ga, Ge, and Se atoms)

The relative energies of the electronic states with different magnetic moments for the pristine hAs and x-substituted hAs (x = B, C, N, O, Ga, Ge, and Se atoms) are listed in Table S1 (ESI†). From the table one can see that only the C- and Ge-substituted hAs in the ground states have a magnetic moment of 1.0 μ_B, while other doped systems, especially the O- and Se-substituted hAs, possess ground states with zero magnetic moment. For these ground states, typical geometric parameters, formation energies, and charge transfer were calculated and are summarized in Table 1. Positive values of formation energies indicate that the formation process of the doped systems is endothermic. Moreover, the values are determined not only by the doped systems, but also by the material states of the doping atoms. In particular, for the x-substituted hAs

Table 1 Typical geometrical parameters, formation energy (E_f), charge transfer (Δq), and magnetic moment (M) for x-substituted hAs (x = B, C, N, O, Ga, Ge, Se, and monovacancy) and x-adsorbed hAs (x = As)

	$d_{x\text{–}As1}$ (Å)	$d_{As1\text{–}As4}$ (Å)	h (Å)	E_f (eV)	Δq (e)	M (μ_B)
B-Substituted hAs	1.97	2.48	0.71	4.67	0.05	0.0
C-Substituted hAs	1.99	2.49	0.82	6.46	0.99	1.0
N-Substituted hAs	2.01	2.50	1.34	0.34	1.15	0.0
O-Substituted hAs	2.02	2.47	1.11	0.64	0.98	0.0
Ga-Substituted hAs	2.43	2.49	1.19	4.02	−0.49	0.0
Ge-Substituted hAs	2.48	2.46	1.22	4.64	−0.31	1.0
Pristine hAs	2.51	2.51	1.39	—	—	0.0
Se-Substituted hAs	2.52	2.46	1.38	4.07	0.27	0.0
Monovacancy-substituted hAs	—	2.47	—	5.04	—	0.0
As-Adsorbed hAs	2.69	2.61	1.82	2.64	0.09	3.0

Published on 01 December 2015. Downloaded by South China University of Technology on 25/02/2016 06:24:13.

(x = N and O atoms), the formation energies are obviously smaller than other systems due to the small energies of x atoms in their molecular gas phase. For the pristine hAs, the As–As bond length and the height of the buckling layer are predicted to be ∼2.51 and 1.39 Å, respectively, in agreement with the values of 2.55 and 1.35 Å calculated by Zhang *et al.* with the GGA/PBE functional.[18] When one As atom in the pristine hAs is substituted by x atoms, the x–As1 bonds (x = B, C, N, O, Ga, Ge, and Se), as shown in Fig. 1, are predicted to be shorter than the As–As bonds of the pristine hAs. Notably, much shorter x–As1 bonds occur in the x-substituted hAs (x = B, C, N, and O) due to small atomic radii and strong electronegativities of the substitutional atoms. Because of the substitutional effect, the As1–As4 bonds in all x-substituted hAs are a little bit longer than the As–As bonds in pristine hAs. Moreover, compared with that between two layers of As atoms in the pristine hAs, the distances between the substitutional atoms and the bottom layer of As atoms clearly become shorter in all x-substituted hAs except for the N-substituted hAs, in which an equivalent distance to the pristine hAs is observed. This equivalent distance should be attributed to the similar hybridization characters between N and As atoms, which facilitate the formation of buckling structures.

Based on the Bader analysis, charge transfer from the substitutional atoms to the monovacancy-hAs is also examined. Compared with the isolated atoms, electron accumulations of about 0.05e, 0.99e, 1.15e, 0.98e, and 0.27e occur at the B, C, N, O and Se atoms, whereas the electron depletions are about 0.49e and 0.31e at the Ga and Ge atoms of the doped hAs, respectively. The electron accumulations and depletions reflect the relative differences in electronegativity of B, C, N, O, Ga, Ge, As, and Se atoms from the As atom. On the other hand, the obvious charge transfers indicate the essential bonding between the substitutional atoms and the As atoms, showing the stability of the doped hAs.

The spin-polarized band structures and PDOS of the pristine and the N-substituted hAs are presented in Fig. 2. For the pristine hAs sheet, the band structures for the up and down spins are the same, as shown in Fig. 2(a), leading to zero magnetic moment. The indirect band gap is estimated to be about 1.6 eV, which is generally consistent with the one calculated by Zhang *et al.* with the GGA/PBE functional.[18] It is clear that the band gap calculated by the GGA/PBE functional is smaller than that calculated by using HSE06, as shown in Fig. S4 (ESI†). This difference in band gap should be attributed to the fact that the GGA/PBE functional usually overestimates electron delocalization, leading to a smaller band gap, while HSE06 may correct this overestimation by partially including the Hartree–Fock (HF) functional, which is known to localize electrons. Remarkably, when one As atom is substituted by one N atom, as shown in Fig. 2(b), the indirect band gap will transform into a direct band gap of 1.3 eV at the Γ point in the Brillouin zone, retaining the spin-unpolarized characteristics. In order to further understand the origin of the valence band (VB) and the conduction band (CB), the spin-polarized PDOS of the pristine and N-substituted hAs sheets are presented in Fig. 2(c) and (d), respectively. It is shown that the VB and CB of the pristine hAs have similar components, *i.e.*, the 4p states coupled with small amounts of the 4s states of As atoms. When one N atom is introduced to substitute an As atom in the supercell of the pristine hAs, no dangling bond appears in the three nearest-neighbor As atoms and no impurity gap states occur in the band gap, which is understandable as the N and As atoms belong to the same family of the V group in the periodic table and have similar hybridization characters.

When one As atom in the pristine hAs is substituted by one x atom (x = B, C, O, Ga, Ge, and Se), obvious impurity gap states occur in the band structures of the x-substituted hAs, as shown in Fig. 3. One can clearly see that similar to the pristine hAs, the B-, Ga-, O-, and Se-substituted hAs are all spin-unpolarized. Nevertheless, when C and Ge atoms are introduced to substitute As atoms, the resultant hAs exhibit typical spin-polarized character. In the B-substituted hAs, the substitutional effect can induce three impurity gap states. One state is occupied, appearing about 0.1 eV above the VB maximum, while another two are unoccupied,

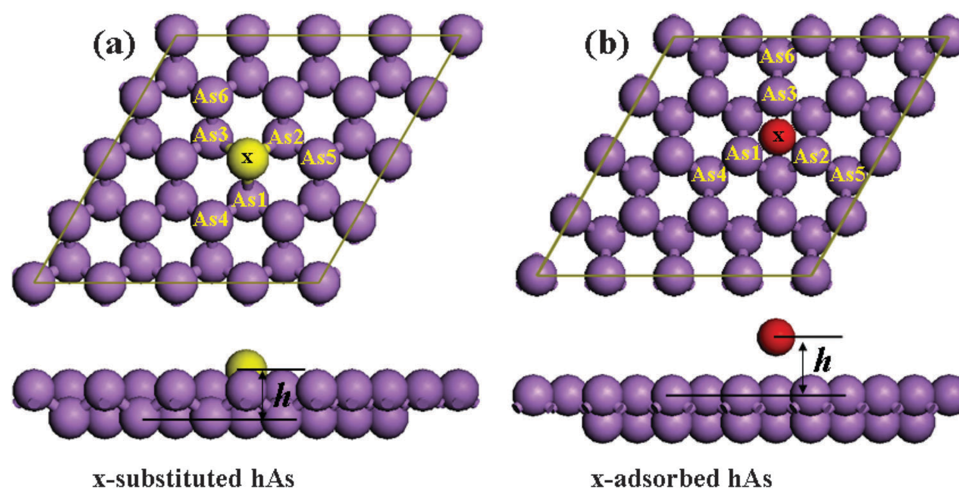

Fig. 1 Top and side views of (a) x-substituted hAs (x = B, C, N, O, Ga, Ge, Se, and monovacancy) and (b) x-adsorbed hAs (x = As). For clarification, the nearest-neighbor As atoms of the dopant x atom are labeled, and other balls represent As atoms in each graph.

This journal is © The Royal Society of Chemistry 2016

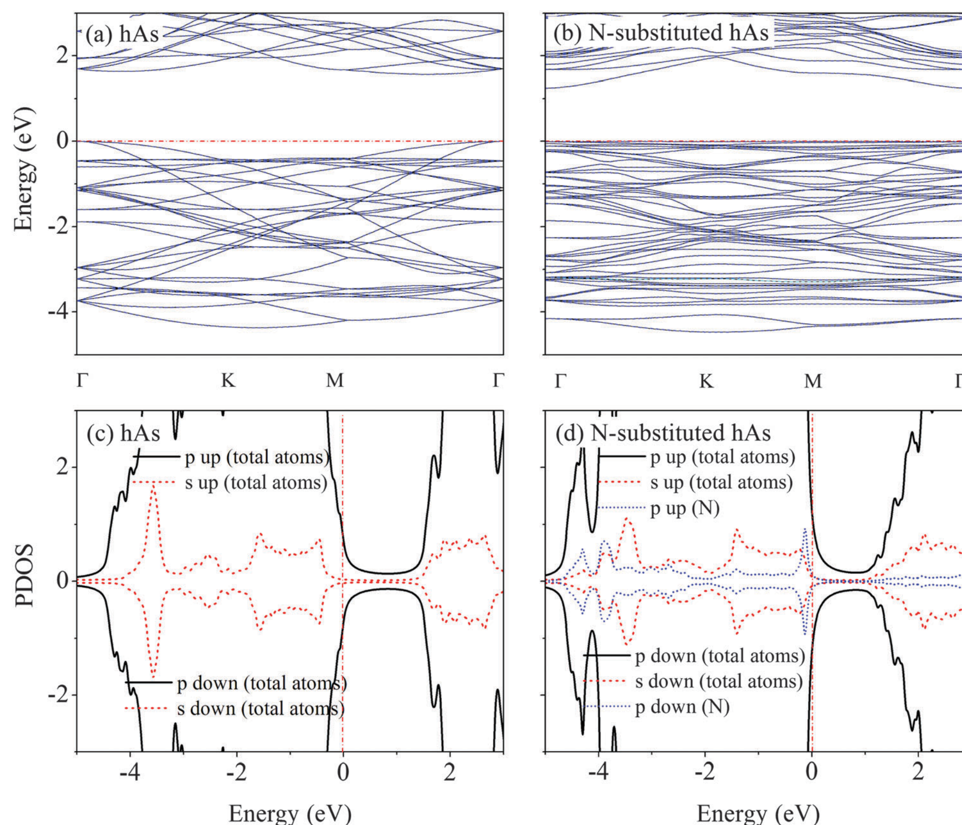

Fig. 2 Spin-polarized band structures and PDOS of the pristine and the N-substituted hAs. Black solid and blue dashed lines in band structures denote spin-up and spin-down channels, respectively. Red dash-dot lines indicate the Fermi level in the band structures and PDOS. To clearly show the delicate contributions from the substitutional atoms near the Fermi level, the range of ordinates in (c) and (d) is set from −3 to 3 eV, and the DOS of the total atoms lies partially outside the range.

Published on 01 December 2015. Downloaded by South China University of Technology on 25/02/2016 06:24:13.

occurring about 0.40 eV below the CB minimum. A direct band gap of about 1.35 eV is observed. In the Ga-substituted hAs, electronic structures similar to the B-substituted system are observed except for an indirect band gap of about 1.25 eV. In the C-substituted hAs, two impurity gap states appear about 0.52 and 1.13 eV above the VB maximum, as shown in Fig. 3(c). Similarly, two impurity gap states occur about 0.45 eV above the VB maximum and about 1.15 eV below the CB minimum in the Ge-substituted hAs, as shown in Fig. 3(d). It should be noted that for both the C- and Ge-substituted systems, the two gap states belong to the up- and down-spin components, respectively. One is occupied and the other is unoccupied, and the Fermi level is located in the gap between these two gap states. The detailed conducting characters of both C- and Ge-substituted hAs sheets will be analyzed according to the PDOS in Fig. 4. Interestingly, when one As atom in the pristine hAs is substituted by one O or one Se atom, as shown in Fig. 3(e) and (f), obvious impurity states crossing the Fermi level are observed, indicative of the metallic characters for both doped systems.

The components of the VB, CB, and impurity gap states and the magnetic properties of the x-substituted hAs (x = B, Ga, C, Ge, O, and Se) are uncovered by the spin-polarized PDOS presented in Fig. 4. It is shown that the VB and CB of the doped systems are primarily composed of the 4p states of As atoms, and the origin of the corresponding impurity gap states are generally complicated. As shown in Fig. 4(a), in the B-substituted hAs, the two occupied gap states consist of the 4p states of the three nearest-neighbor As1, As2 and As3 atoms, whereas the unoccupied gap states are primarily contributed by the 2p states of B atom coupled with a small amount of the 4p states of the three nearest-neighbor As1, As2, and As3 atoms. These impurity states decrease the band gaps. Similar cases are also observed in Fig. 4(b) for the Ga-substituted hAs. Since the hybridizations between the substitutional atoms and the As atoms are very weak, these two doped systems retain the spin-unpolarized characters.

The PDOS in Fig. 4(c) and (d) show that in the impurity gap states of the C- and Ge-substituted hAs, there are almost equivalent contributions from the 2p states of the C atom and the 4p states of the three nearest-neighbor atoms As1, As2, and As3, indicating strong orbital hybridizations between the C atom and its nearest-neighbor As atoms. Unlike the B-, N-, and Ga-substituted hAs, the strong hybridizations cause the splitting of the bands between the spin-up and spin-down channels near the Fermi level in the impurity gap states of the C- and Ge-substituted hAs. Due to these splittings, the C- and Ge-substituted hAs exhibit spin-polarized semiconducting characters with band gaps of 1.1 and 1.3 eV for the spin-up

Published on 01 December 2015. Downloaded by South China University of Technology on 25/02/2016 06:24:13.

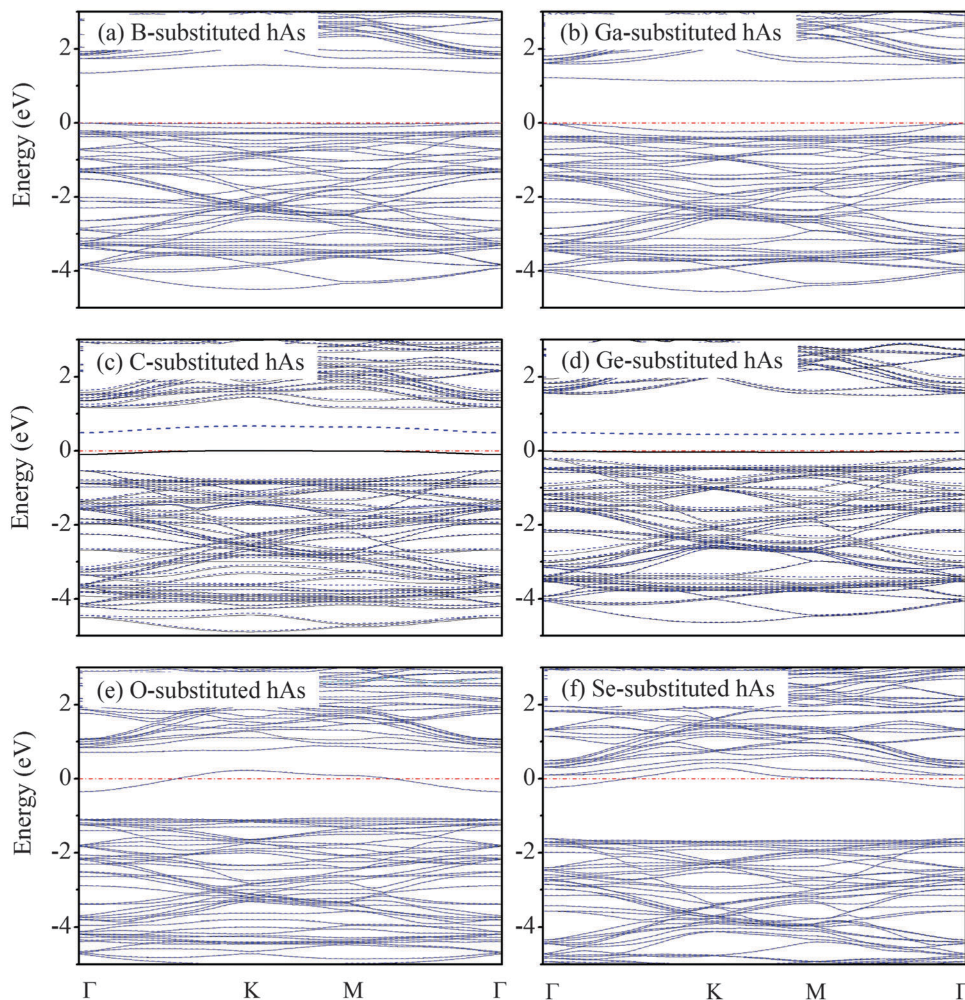

Fig. 3 Spin-polarized band structures of (a) B-substituted, (b) Ga-substituted, (c) C-substituted, (d) Ge-substituted, (e) O-substituted, and (f) Se-substituted hAs. Black solid and blue dashed lines denote spin-up and spin-down channels and red dash-dot lines indicate the Fermi level, respectively.

channels, and with band gaps of 1.0 and 0.7 eV for the spin-down channels, respectively. Moreover, for these two doped systems, the band gaps between the spin-up VB and spin-down CB are 0.35 and 0.25 eV, respectively. The splitting between spin-up and spin-down channels induces a magnetic moment of 1.0 μ_B in the C- and Ge-substituted hAs, as shown by the data in Table 1. To further understand the origin of the magnetic moments, the spin densities were calculated for the C- and Ge-substituted hAs. For simplicity, only spin density image for the C-substituted hAs is presented in Fig. 5(a). One can see that the spin density is mainly localized at the substitutional C atom and its nearest-neighbor As atoms, consistent with the observation in the PDOS presented in Fig. 4(c).

For the metallic O-substituted hAs with an impurity gap state crossing the Fermi level, its gap states are dominated by the 4p states of the three nearest-neighbor atoms As1, As2, and As3, and the contribution from the substitutional O atom is too small so as to be negligible, as shown in Fig. 4(e). Therefore, the O-substituted hAs exhibits spin-unpolarized metallicity, different from the C- and Ge-substituted systems with a net magnetic moment of 1.0 μ_B. Although no obvious impurity gap state occurs in the Se-substituted hAs, the Fermi level crosses the CB minimum, and the doped system is thus metallic as well with spin-unpolarized character, as shown in Fig. 4(f). To further give some insight into the spin-unpolarized character of O- and Se-substituted hAs, we compared their PDOS with those of the C- and Ge-substituted systems. It can be seen from Fig. 4(c–f) that in the O- and Se-substituted hAs the p electrons of the O and Se atoms are more delocalized than those of C- and Ge atoms in the C- and Ge-substituted systems, especially near the Fermi level. Therefore, in view of the poor hybridization between the substituted atoms of O and Se and the three nearest-neighbor As atoms, the O- and Se-substituted hAs should have zero magnetic moment.

From the above discussion one can see that, in general, the doped hAs, in which the doping atoms belong to the same group in the periodic table, show virtually similar electronic structures and magnetic properties due to their similar electronic structures. However, they can have different geometrical parameters, formation energies, and charge transfer mainly due to different

This journal is © The Royal Society of Chemistry 2016

Published on 01 December 2015. Downloaded by South China University of Technology on 25/02/2016 06:24:13.

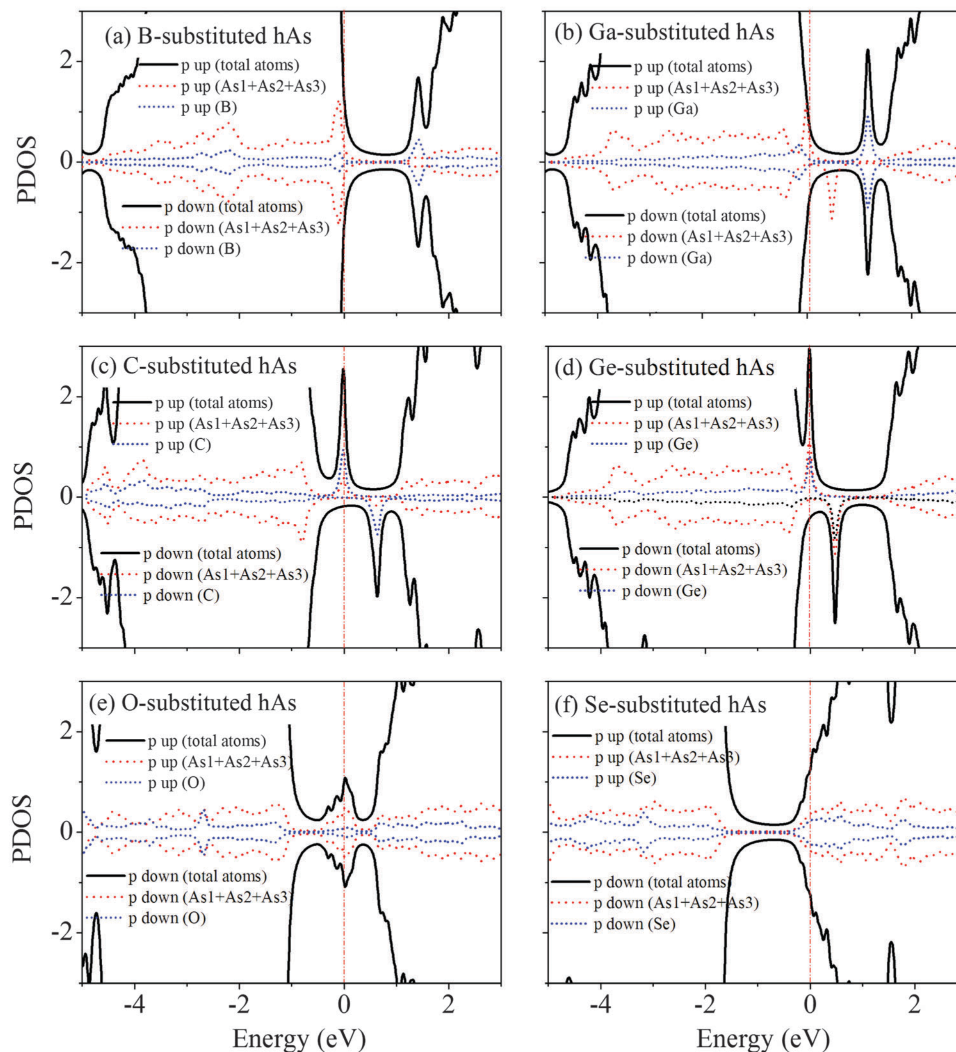

Fig. 4 Spin-polarized PDOS of (a) B-substituted, (b) Ga-substituted, (c) C-substituted, (d) Ge-substituted, (e) O-substituted, and (f) Se-substituted hAs. Red dash-dot lines indicate the Fermi level. To clearly show the delicate contributions from the substitutional atoms near the Fermi level, the range of ordinates is set from −3 to 3 eV, and the DOS of total atoms lies partially outside the range.

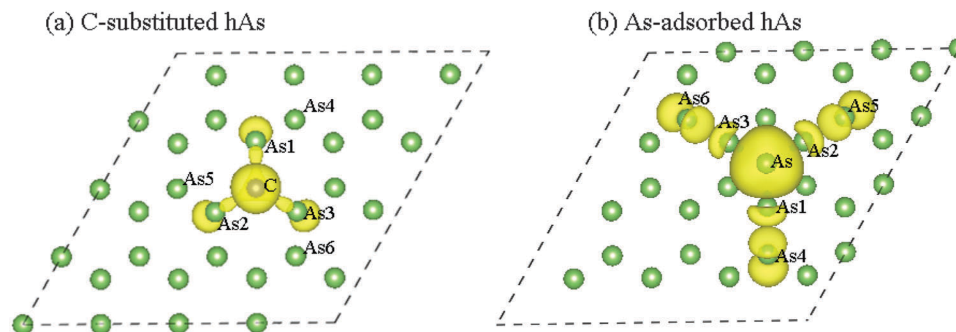

Fig. 5 Spin density images for (a) C-substituted (b) As-adsorbed hAs. The substitutional C, the adsorbed As, and their nearest-neighbor As atoms are labeled, and other balls without special labels represent As atoms.

atomic radii and electronegativities. What is more, for the doped systems in which the doping atoms belong to different groups, obviously different properties were observed. For example, it is expected that the B- and Ga-substituted hAs with even electrons are spin-unpolarized and the C- and Ge-substituted hAs with odd electrons have typical spin-polarized characteristics with a magnetic moment of 1.0 μ_B. However, spin-unpolarized characteristics were observed in the O- and Se-substituted systems

Published on 01 December 2015. Downloaded by South China University of Technology on 25/02/2016 06:24:13.

with odd electrons due to the delocalization of p electrons in the doping atoms O and Se.

3.2 Monovacancy-substituted and As-adsorbed hAs

Besides atom-substitution doping, the influence of vacancies and the adsorption of As atoms on the electronic structures of hAs were also investigated since these two types of impurities may occur in the preparation of hAs. There is one configuration for monovacancy-substituted doping in the supercell. For the adsorption of an As atom on the surface of the pristine hAs, two configurations are considered. One is the top configuration in which the adsorbed As atom is on the top site of the As atoms, the other is the hollow configuration in which the As atom is on the hollow site of the pristine hAs. The total energy calculations indicate that the hollow configuration is more stable. Thus only this configuration, as shown in Fig. 1(b), is further studied.

For the monovacancy-substituted and the As-adsorbed hAs, the geometric parameters, formation energy, and charge transfer are presented in Table 1. The formation energies calculated indicate that the formation of the monovacancy-substituted and As-adsorbed hAs are endothermic processes. In the monovacancy-substituted hAs, the As1–As4 bond becomes shorter than that in the pristine hAs. To evaluate the strength of the bond between the adsorbed As atom and the hAs sheet, the adsorption energy was calculated using the formula $E_a = E_{complex} - (E_{hAs} + E_x)$, where $E_{complex}$ and E_{hAs} are the total energies of the As-adsorbed hAs and pristine hAs sheets, and E_x is the energy of the isolated As atom. The calculated adsorption energy of −0.34 eV indicates that the As atom can be chemically adsorbed on the hAs sheet. What is more, the distance between the absorbed atom of As and the top As layer of hAs is about 1.82 Å, and the length of the As–As1 bond is about 2.69 Å, further indicating chemical bonding interaction between the adsorbed As atom and the As1, As2, and As3 atoms, respectively. In fact, these chemical bonding was further confirmed by Bader charge analysis, which reveals electron accumulation of about 0.09e at the absorbed As atom. Detailed discussion of the bonding interaction will be given afterwards.

The spin-polarized band structures and the PDOS of the monovacancy-substituted and As-adsorbed hAs are presented in Fig. 6. One can see from Fig. 6(a) that the band structures of the up- and down-spin components are virtually identical. Two impurity gap states are induced by the monovacancy substitution. One is partially occupied and the other is unoccupied, and the doped system is metallic. The symmetry of the PDOS in the spin-up and spin-down channels in Fig. 6(c) shows that the gap states are mainly contributed from the 4p states of the three nearest-neighbor As1, As2, and As3 atoms. In view of the absence of one As atom, the nature of these gap states should be associated with the dangling bonds of the As1, As2, and As3 atoms.

In contrast, the adsorption of an As atom on the surface of the pristine hAs causes the formation of six impurity gap states, as shown in Fig. 6(b). One state is occupied, two are partially occupied, and the other three are unoccupied. The former three

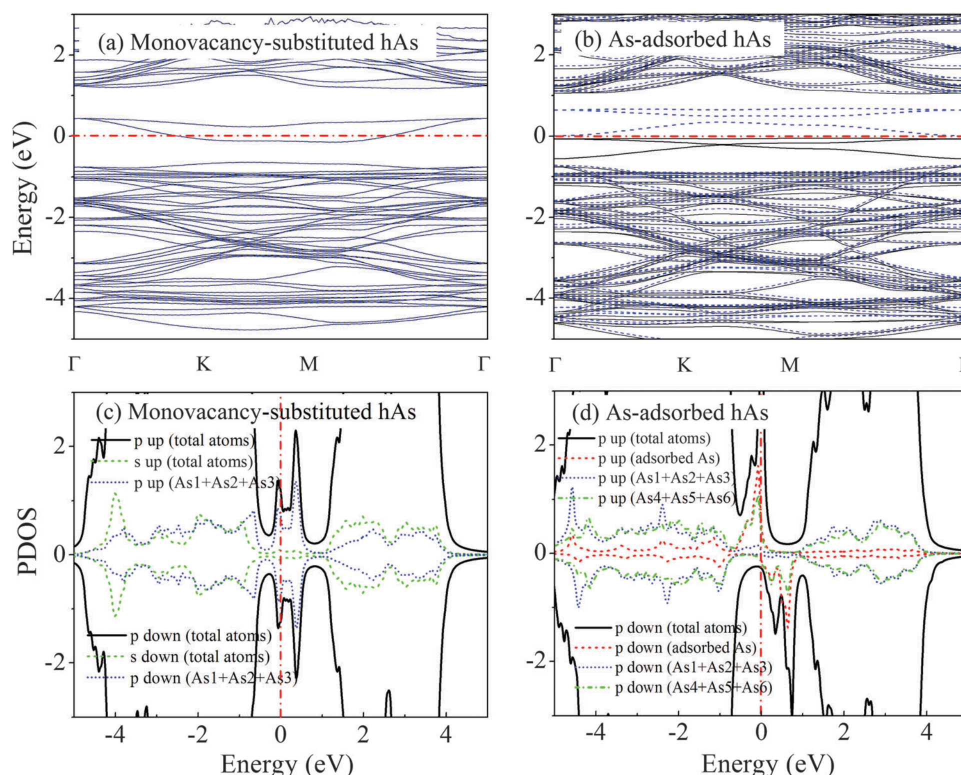

Fig. 6 Spin-polarized band structures and PDOS of the monovacancy-substituted and As-adsorbed hAs. Black solid and blue dashed lines in band structures denote spin-up and spin-down channels, respectively. Red dash-dot lines indicate the Fermi level in the band structures and PDOS. To clearly show the delicate contributions from the substitutional atoms near the Fermi level, the range of ordinates is all set from −3 to 3 eV, and the DOS of the total atoms lies partially outside the range.

 This journal is © The Royal Society of Chemistry 2016

Published on 01 December 2015. Downloaded by South China University of Technology on 25/02/2016 06:24:13.

states belong to the spin-up components and the latter three are spin-down ones. On the one hand the PDOS in Fig. 6(d) indicates that the energy level splits near the Fermi level between the spin-up and spin-down channels. The spin-up component crosses the Fermi level and yields metallic character while the spin-down channel remains semiconducting. The energy splitting near the Fermi level induces a magnetic moment of about 3.0 μ_B, as listed in Table 1. In light of this, the As-adsorbed hAs is half-metallic. On the other hand, the PDOS in Fig. 6(d) shows that the origin of these impurity gap states is mainly the hybridization of the 4p states of the adsorbed As atoms and those of the next-nearest-neighbor atoms As4, As5, and As6, as labeled in Fig. 1(b). In comparison, the contributions from the 4p states of the three nearest-neighbor As1, As2, and As3 atoms are small. Therefore, the magnetic moment can be attributed to the contribution from the hybridization between the 4p states of the adsorbed As atoms and that of its next-nearest-neighbor As atoms. These results are unexpected and interesting because the adsorbed As atom is bonded not directly with the As4, As5, and As6 atoms, but with the three nearest-neighbor atoms of As1, As2, and As3.

To further understand the above unexpected results in the As-adsorbed hAs, the bonding characters are analyzed on the basis of the spin density image, as shown in Fig. 5(b). According to the PDOS in Fig. 6(d), the spin polarization only occurs near the Fermi level, thus the spin electron density distributions can reflect the contributions of different atoms to the impurity gap states. It can be seen from Fig. 5(b) that the spin density is mainly localized at the adsorbed As atom and its next-nearest-neighboring atoms As4, As5 and A6, whereas those at the three nearest-neighbor atoms As1, As2 and As3 are too small. This observation is consistent with the results observed in the PDOS. On the other hand, the distance of 2.69 Å and the electron accumulation of about 0.09e on the adsorbed As atom indicate the essential bonding between the adsorbed As atom and the three nearest-neighbor atoms As1, As2, and As3, as listed in Table 1. Because the bonding between the adsorbed As atom and its nearest-neighbor As1, As2, and As3 atoms lies on the same lines with the As1–As4, As2–As5, and As3–As6 bonds, these bonding interactions consequentially weaken the latter three bonds. As a result, the corresponding bond lengths consequently become larger than the ones in the pristine hAs, as indicated by the data in Table 1. Understandably, due to the weakened As1–As4, As2–As5, and As3–As6 bonds, the charge distributions on the As4, As5, and As6 atoms become localized toward the Fermi level, leading to the metallic behavior of the As-adsorbed hAs.[16]

4. Conclusions

In summary, we have theoretically investigated and reported on the electronic and magnetic properties of x-substituted hAs (x = B, C, N, O, Ga, Ge, Se, and monovacancy) and x-adsorbed hAs (x = As). The B-, N-, and Ga-substituted hAs retain semiconducting characters similar to the pristine hA except for the transition from indirect to direct band gaps in the former two doped systems due to the influence of the impurity gap states. In contrast, the O-, Se-, and monovacancy-substituted hAs sheets exhibit typical metallic behavior, and the C- and Ge-substituted hAs show spin-polarization semiconducting character with band gaps of 1.1 and 1.3 eV for the spin-up channels and 1.0 and 0.7 eV for the spin-down channels, respectively. For the As-adsorbed hAs, the Fermi level crosses the spin-up states, yielding metallic character, while the spin-down channel remains semiconducting. For the spin-polarized systems, a further analysis of electronic structures indicates that the hybridization between the doping atoms and the As atoms results in an energy splitting near the Fermi level and consequently induces magnetic moments. We have explicitly demonstrated that the conducting characters of hAs can be easily tuned from a spin-nonpolarized semiconductor, to a spin-polarized semiconductor, to a metal, or to a half-metal by selective impurity doping, suggesting its promising applications in future electronics, spintronics, and optoelectronics.

Acknowledgements

This work was supported by the Natural Science Foundation of China (NSFC, No. 61575059, 21101051, 11474100), the Anhui Provincial Natural Science Foundation (No. 1408085MA18), the Fundamental Research Funds for the Central Universities (2012HGCX0003, 2013HGCH0012, 2014HGCH0005, JZ2015-HGXJ0184, 2015PT017), and the Key Research Foundation of Anhui Provincial Educational Committee (KJ2015A040).

References

1 K. S. Novoselov, A. K. Geim, S. V. Morozov, D. Jiang, Y. Zhang, S. V. Dubonos, I. V. Grigorieva and A. A. Firsov, *Science*, 2004, **306**, 666–669.
2 K. S. Novoselov, A. K. Geim, S. V. Morozov, D. Jiang, M. I. Katsnelson, I. V. Grigorieva, S. V. Dubonos and A. A. Firsov, *Nature*, 2005, **438**, 197–200.
3 P. Vogt, P. De Padova, C. Quaresima, J. Avila, E. Frantzeskakis, M. C. Asensio, A. Resta, B. Ealet and G. Le Lay, *Phys. Rev. Lett.*, 2012, **108**, 155501.
4 G. G. Guzman-Verri and L. C. L. Y. Voon, *Phys. Rev. B: Condens. Matter Mater. Phys.*, 2007, **76**, 075131.
5 C. H. Jin, F. Lin, K. Suenaga and S. Iijima, *Phys. Rev. Lett.*, 2009, **102**, 195505.
6 J. C. Meyer, A. Chuvilin, G. Algara-Siller, J. Biskupek and U. Kaiser, *Nano Lett.*, 2009, **9**, 2683–2689.
7 L. Song, L. Ci, H. Lu, P. B. Sorokin, C. Jin, J. Ni, A. G. Kvashnin, D. G. Kvashnin, J. Lou, B. I. Yakobson and P. M. Ajayan, *Nano Lett.*, 2010, **10**, 3209–3215.
8 K. K. Liu, W. J. Zhang, Y. H. Lee, Y. C. Lin, M. T. Chang, C. Su, C. S. Chang, H. Li, Y. M. Shi, H. Zhang, C. S. Lai and L. J. Li, *Nano Lett.*, 2012, **12**, 1538–1544.
9 Y. Zhang, T. R. Chang, B. Zhou, Y. T. Cui, H. Yan, Z. K. Liu, F. Schmitt, J. Lee, R. Moore, Y. L. Chen, H. Lin, H. T. Jeng,

View Article Online

Published on 01 December 2015. Downloaded by South China University of Technology on 25/02/2016 06:24:13.

S. K. Mo, Z. Hussain, A. Bansil and Z. X. Shen, *Nat. Nanotechnol.*, 2014, **9**, 111–115.

10 X. Huang, Z. Y. Zeng and H. Zhang, *Chem. Soc. Rev.*, 2013, **42**, 1934–1946.

11 H. Liu, Y. C. Du, Y. X. Deng and P. D. Ye, *Chem. Soc. Rev.*, 2015, **44**, 2732–2743.

12 J. Na, Y. T. Lee, J. A. Lim, D. K. Hwang, G. T. Kim, W. K. Choi and Y. W. Song, *ACS Nano*, 2014, **8**, 11753–11762.

13 D. Cakir, H. Sahin and F. M. Peeters, *Phys. Rev. B: Condens. Matter Mater. Phys.*, 2014, **90**, 205421.

14 B. Radisavljevic, A. Radenovic, J. Brivio, V. Giacometti and A. Kis, *Nat. Nanotechnol.*, 2011, **6**, 147–150.

15 H. Liu, J. Gu and P. D. Ye, *IEEE Electron Device Lett.*, 2012, **33**, 1273–1275.

16 B. Nie, J. G. Hu, L. B. Luo, C. Xie, L. H. Zeng, P. Lv, F. Z. Li, J. S. Jie, M. Feng, C. Y. Wu, Y. Q. Yu and S. H. Yu, *Small*, 2013, **17**, 2872–2879.

17 H. L. Zeng, J. F. Dai, W. Yao, D. Xiao and X. D. Cui, *Nat. Nanotechnol.*, 2012, **7**, 490–493.

18 S. Zhang, Z. Yan, Y. Li, Z. Chen and H. Zeng, *Angew. Chem., Int. Ed.*, 2015, **54**, 3112–3115.

19 C. Kamal and M. Ezawa, *Phys. Rev. B: Condens. Matter Mater. Phys.*, 2015, **91**, 085423.

20 L. Kou, Y. Ma, X. Tan, T. Frauenheim, A. Du and S. Smith, *J. Phys. Chem. C*, 2015, **119**, 6918–6922.

21 Y. Wang and Y. Ding, *Nanoscale Res. Lett.*, 2015, **10**, 955.

22 Y. Wang and Y. Ding, *J. Phys.: Condens. Matter*, 2015, **27**, 225304–225314.

23 S. Zhang, Y. Hu, Z. Hu, B. Cai and H. Zeng, *Appl. Phys. Lett.*, 2015, **107**, 022102.

24 Y. H. Hu, S. L. Zhang, S. F. Sun, M. Q. Xie, B. Cai and H. B. Zeng, *Appl. Phys. Lett.*, 2015, **107**, 122107.

25 K. Dolui, I. Rungger, C. Das Pemmaraju and S. Sanvito, *Phys. Rev. B: Condens. Matter Mater. Phys.*, 2013, **88**, 075420.

26 A. Ramasubramaniam and D. Naveh, *Phys. Rev. B: Condens. Matter Mater. Phys.*, 2013, **87**, 195201.

27 J. S. Qi, X. Li, X. F. Chen and K. G. Hu, *J. Phys.: Condens. Matter*, 2014, **26**, 256003.

28 X. X. Li, J. Zhao and J. L. Yang, *Sci. Rep.*, 2013, **3**, 1858.

29 Y. G. Zhou, J. Xiao-Dong, Z. G. Wang, H. Y. Xiao, F. Gao and X. T. Zu, *Phys. Chem. Chem. Phys.*, 2010, **12**, 7588–7592.

30 F. Wu, E. J. Kan, H. J. Xiang, S. H. Wei, M. H. Whangbo and J. L. Yang, *Appl. Phys. Lett.*, 2009, **94**, 223105.

31 L. B. Luo, X. B. Yang, F. X. Liang, J. S. Jie, C. Y. Wu, L. Wang, Y. Q. Yu and Z. F. Zhu, *J. Phys. Chem. C*, 2011, **115**, 24293–24299.

32 L. B. Luo, X. B. Yang, F. X. Liang, J. S. Jie, Q. Li, Z. F. Zhu, C. Y. Wu, Y. Q. Yu and L. Wang, *CrystEngComm*, 2012, **14**, 1942–1947.

33 P. E. Blochl, *Phys. Rev. B: Condens. Matter Mater. Phys.*, 1994, **50**, 17953–17979.

34 G. Kresse and J. Furthmuller, *Comput. Mater. Sci.*, 1996, **6**, 15–50.

35 G. Kresse and D. Joubert, *Phys. Rev. B: Condens. Matter Mater. Phys.*, 1999, **59**, 1758–1775.

36 J. P. Perdew, K. Burke and M. Ernzerhof, *Phys. Rev. Lett.*, 1996, **77**, 3865–3868.

37 G. Henkelman, A. Arnaldsson and H. Jonsson, *Comput. Mater. Sci.*, 2006, **36**, 354–360.

This journal is © The Royal Society of Chemistry 2016